J Biomol NMR (2009) 43:121–129
DOI 10.1007/s10858-008-9293-8

COMMUNICATION

Measurement of imino ^{1}H–^{1}H residual dipolar couplings in RNA

Michael P. Latham · Arthur Pardi

Received: 16 September 2008 / Accepted: 13 November 2008 / Published online: 9 December 2008

Abstract Imino ^{1}H–^{15}N residual dipolar couplings (RDCs) provide additional structural information that complements standard ^{1}H–^{1}H NOEs leading to improvements in both the local and global structure of RNAs. Here, we report measurement of imino ^{1}H–^{1}H RDCs for the Iron Responsive Element (IRE) RNA and native *E. coli* $tRNA^{Val}$ using a BEST-Jcomp-HMQC2 experiment. ^{1}H–^{1}H RDCs are observed between the imino protons in G–U wobble base pairs and between imino protons on neighboring base pairs in both RNAs. These imino ^{1}H–^{1}H RDCs complement standard ^{1}H–^{15}N RDCs because the ^{1}H–^{1}H vectors generally point along the helical axis, roughly perpendicular to ^{1}H–^{15}N RDCs. The use of longitudinal relaxation enhancement increased the signal-to-noise of the spectra by ~3.5-fold over the standard experiment. The ability to measure imino ^{1}H–^{1}H RDCs offers a new restraint, which can be used in NMR domain orientation and structural studies of RNAs.

Keywords Residual dipolar couplings · RNA structure · Partial alignment · tRNA · Iron responsive element RNA

Solution NMR studies of nucleic acids are more challenging than those of similarly sized proteins due to the lower proton density and more extended structures generally found in nucleic acids. As a result, the local structure of nucleic acids can often be well-determined from NOE and J-coupling constant restraints, whereas the global orientations of helical secondary structural elements are usually much less precisely determined (Vermeulen et al. 2000). Residual dipolar coupling (RDC) data relate internuclear vectors to a common molecular axis system (Bothner-By et al. 1981; Kung et al. 1995; Tolman et al. 1995; Bax et al. 2001), and provide long-range global information that complements short-range NOE and J-coupling constants. Thus, RDC constraints obtained under conditions of weak alignment (Tjandra and Bax 1997) are extremely valuable for NMR solution structure determination of nucleic acids (Hansen et al. 2000; Mollova and Pardi 2000; Lukavsky et al. 2003; Davis et al. 2005).

The vast majority of RDCs routinely measured in biomolecules involve interactions between nuclei at a fixed known distance (Bax et al. 2001; Prestegard et al. 2004). The most commonly measured RDCs in nucleic acids are the ^{1}H–^{15}N iminos of guanine and uracil, the $^{1}H2$–$^{13}C2$ of adenine, the $^{1}H8$–$^{13}C8$ of purines, the $^{1}H6$–$^{13}C6$ and $^{1}H5$–$^{13}C5$ of pyrimidines, and the $^{1}H1'$–$^{13}C1'$ of the ribose sugar. Experiments have also been developed to measure additional RDCs in nucleic acids, for example between other nuclei separated by one- and two-bonds in the nucleobase and ribose-phosphate backbone (Fiala et al. 2004; Latham et al. 2005; Getz et al. 2007). Of all these nuclei, the imino protons generally offer the highest resolution, and thus represent important probes for collecting structural restraints.

Imino ^{1}H–^{15}N RDCs have previously been used in domain orientation studies of helical regions in RNAs

Electronic supplementary material The online version of this article (doi:10.1007/s10858-008-9293-8) contains supplementary material, which is available to authorized users.

M. P. Latham · A. Pardi (✉)
Department of Chemistry and Biochemistry, 215 UCB, University of Colorado, Boulder, CO 80309-0215, USA
e-mail: arthur.pardi@colorado.edu

Present Address:
M. P. Latham
Department of Molecular Genetics, University of Toronto, Toronto, ON M5S 1A8, Canada

(Mollova et al. 2000; Al-Hashimi et al. 2002; Bondensgaard et al. 2002; Lukavsky et al. 2003; D'Souza et al. 2004; Vermeulen et al. 2005; Getz et al. 2007; Ying et al. 2007); however, there is generally only one imino ^{1}H–^{15}N RDC for each base pair in helical regions leading to few restraints. Thus, ^{1}H–^{1}H RDCs (D_{HH}) between the well-resolved imino protons represent attractive candidates for providing additional structural data. The high proton gyromagnetic ratio can yield large residual dipolar couplings (Hansen et al. 1998b; Lipsitz and Tjandra 2004), so various methods have been developed for measuring D_{HH} values to take advantage of these additional structural constraints (Hansen et al. 1998b; Tian et al. 2000; Wu and Bax 2002; Boisbouvier et al. 2003; Meier et al. 2003). However, a major obstacle in these measurements is the large network of simultaneously dipolar coupled ^{1}H probes in the biomolecule, making the measurement of D_{HH} values greater than 4 Å apart difficult (Hansen et al. 1998a, b). Strategies for perdeuteration and/or homonuclear decoupling have therefore been developed to help overcome these problems (Scott et al. 2000; Tian et al. 2000; Wu and Bax 2002; Boisbouvier et al. 2003; Meier et al. 2003). For example, homonuclear decoupling methods have been used to measure D_{HH} values between the non-exchangeable H1′ resonances to help improve the accuracy and precision of a DNA duplex structure (Boisbouvier et al. 2003). Bax and co-workers used a semi-selective pulse sequence to measure ^{1}H–^{1}H RDCs between amide protons in proteins (Wu and Bax 2002). This so-called SS-HMQC2 pulse sequence consists of two semi-selective heteronuclear multiple quantum coherence (HMQC) blocks surrounding a COSY-type mixing pulse, and the magnitudes of D_{HH} are determined from a quantitative J-correlation type approach (Wu and Bax 2002). Recently, Schanda et al. (2007) employed modifications to this experiment, which resulted in 1.5–8 times higher signal-to-noise for measurement of amide ^{1}H–^{1}H RDCs in proteins. This experiment is referred to as BEST-Jcomp-HMQC2, where BEST stands for: Band-selective-Excitation Short-Transient and Jcomp for: J-mismatch compensated (Schanda et al. 2007). The higher sensitivity is the result of two improvements: longitudinal relaxation enhancement (Pervushin et al. 2002; Schanda and Brutscher 2005; Schanda et al. 2005) and J-mismatch compensation (Schanda et al. 2007). Here, we report the application of this BEST-Jcomp-HMQC2 technique for measuring D_{HH} interactions between the well-resolved imino protons in ^{15}N-labeled RNAs.

The original 2D ^{15}N–^{1}H BEST-Jcomp-HMQC2 experiment (Schanda et al. 2007) was modified here so proton evolution occurs during the t_1 period allowing for measurement of D_{HH} couplings in a spectrum analogous to a 2D ^{1}H–^{1}H NOESY data set (Supplementary Fig. 1). In addition to increasing the sensitivity, the ^{1}H selective pulses employed by the BEST approach only excite the exchangeable imino protons; whereas, the other protons remain at equilibrium. This ensures that D_{HH} evolve between imino protons and not between imino and neighboring amino protons, which are close together in a base pair (~1.9–2.5 Å). The modified BEST-Jcomp-HMQC2 experiment was performed on a 1 mM uniformly ^{15}N-labeled IRE RNA (inset of Fig. 1) sample containing ~17 mg/ml Pf1 bacteriophage (McCallum and Pardi 2003). Figure 1 shows the imino proton region of the 2D ^{1}H–^{1}H BEST-Jcomp-HMQC2 spectrum collected at 25°C on a 600 MHz instrument equipped with a cryogenically cooled probe using HMQC constant time delays of $\Delta_1 = \Delta_2 = 35$ ms (Supplementary Fig. 1), an inter-scan delay of 0.69 s and 400 scans per FID for a total experiment time of 45 h. As expected, the selective excitation results in only couplings between the imino groups with no other peaks observed in the spectrum (data not shown). The strongest cross peaks in the BEST-Jcomp-HMQC2 spectrum arise from imino protons in the G25–U5 wobble base pair, where the two imino protons are separate by ~3.1 Å (McCallum and Pardi 2003). Cross peaks are also observed for the G22–U9 base pair (~2.2 Å imino proton distance), and the remaining cross peaks in Fig. 1 involve imino protons on neighboring base pairs in the IRE. Some non-linear phase error is observed in the indirect ^{1}H dimension, possibly due the selective pulses; however, it is still possible to obtain precise values for the imino ^{1}H–^{1}H RDC (see below).

The absolute value of D_{HH} ($|D_{HH}|$) was calculated from the ratio of cross (I^{AB}_{cross} and I^{BA}_{cross}) and diagonal peak (I^{AA}_{diag} and I^{BB}_{diag}) intensities according to the following equation (Wu and Bax 2002; Schanda et al. 2007):

$$\frac{I^{AB}_{cross} I^{BA}_{cross}}{I^{AA}_{diag} I^{BB}_{diag}} = \frac{\lambda^2 \sin^2(\pi D_{HH}\Delta_1)\sin^2(\pi D_{HH}\Delta_2)}{\lambda^2 \cos^2(\pi D_{HH}\Delta_1)\cos^2(\pi D_{HH}\Delta_2) + 2\lambda(1-\lambda)\cos(\pi D_{HH}\Delta_1)\cos(\pi D_{HH}\Delta_2) + (1-\lambda)^2} \quad (1)$$

where Δ_1 and Δ_2 are the constant time delays for the first and second HMQC blocks ($\Delta_1 = \Delta_2 = 35$ ms), respectively, and λ is a correction for the percentage of protonation versus deuteration at each imino residue

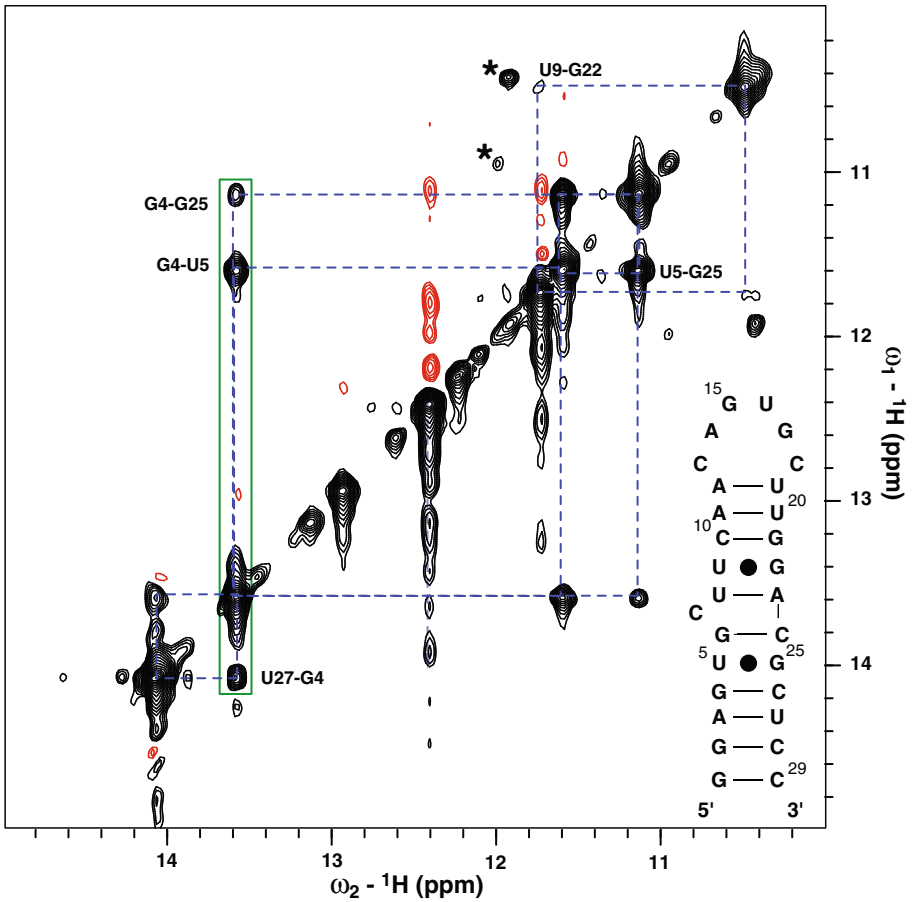

Fig. 1 Imino region of the 2D ^{1}H–^{1}H BEST-Jcomp-HMQC2 experiment (Schanda et al. 2007) shown in Supplemental Fig. 1 collected on a 1 mM ^{15}N-labeled IRE RNA containing ~17 mg/ml Pf1 bacteriophage. This spectrum was collected on a Varian INOVA 600 MHz spectrometer equipped with a cryogenically cooled triple resonance *z*-axis gradient probe operating at 25°C. HMQC constant time delays were $\Delta_1 = \Delta_2 = 35$ ms. 140 × 2,048 complex points were taken using sweep widths of 14,006 Hz in the t_1 and t_2 dimensions. 400 scans per FID were collected with a 0.69 s inter-scan delay for a total experiment time of ~45 h. Black and red contours represent positive and negative intensity, respectively. The dashed blue lines illustrate the cross peaks which arise because of the transfer of magnetization due to imino ^{1}H–^{1}H RDCs. The asterisks denote cross peaks for the two G–U wobble base pairs, which are in an alternate conformation. The previously published imino assignments are indicated (Addess et al. 1997), and the sequence and secondary structure of the IRE are shown in the lower right

($\lambda = 0.95$ for this IRE NMR sample) (Wu and Bax 2002). The intensity ratios and experimental $|D_{HH}|$ values for the data set shown in Fig. 1 are reported in Table 1. Error estimates in the intensity ratios and experimental $|D_{HH}|$ values were obtain from triplicate BEST-Jcomp-HMQC2 experiments. Two additional data sets were collected at 500 MHz at 25°C with a room temperature probe using the same numbers of complex points in both dimensions as the 600 MHz data set, an inter-scan delay of 0.8 s and 256 scans per FID for a total experiment time of 20 h (data not shown). The average standard deviation of 0.1 Hz for the $|D_{HH}|$ values indicates a high level of precision.

The experimental $|D_{HH}|$ values were compared to $|D_{HH}|$ values predicted from the previously RDC-refined NMR solution structure for the IRE (Table 1) using the REDCAT program (Valafar and Prestegard 2004). The alignment tensor used for these predictions was determined from the experimental ^{1}H–^{15}N RDCs for the IRE (McCallum and Pardi 2003). Figure 2 shows the plot of the predicted versus experimental (600 MHz and average values) imino ^{1}H–^{1}H RDCs. The 600 MHz data have a Pearson's correlation coefficient (R_P) of 0.99 and fit well to the RDC-refined solution structure: average rmsd = 0.35 Hz and Q-factor = 0.11 (Cornilescu et al. 1998). The largest experimental $|D_{HH}|$ (5.4 Hz) was between the imino protons in the G25–U5 base pair and the next largest $|D_{HH}|$ (3.7 Hz) was for the inter-base pair G4–U5 interaction. The smallest magnitude imino-imino D_{HH} that was observed in the IRE was between the imino protons of G4–G25 (1.9 Hz). The smaller experimental than predicted D_{HH} value for the G22–U9 interaction results from overlap of the U9 diagonal peak with the imino resonance of G21 (see

Table 1 Experimental and predicted imino ^{1}H–^{1}H RDCs for ^{15}N-labeled IRE RNA containing ~17 mg/ml Pf1 phage

Imino assignment[a]	$\frac{I^{AB}_{cross} I^{BA}_{cross}}{I^{AA}_{diag} I^{BB}_{diag}} (\times 10^{-3})$[b]	Experimental $\lvert D_{HH}\rvert$ (Hz)[c]	Predicted $\lvert D_{HH}\rvert$ (Hz)[d]	Internuclear distance (Å)[e]
U27–G4	3.6 ± 1.7	2.3 ± 0.2	2.3	3.3
G4–U5	27 ± 4.8	3.7 ± 0.1	3.5	3.2
G4–G25	1.7 ± 0.6	1.9 ± 0.1	1.5	4.0
G25–U5	160 ± 30	5.4 ± 0.1	5.5	3.1
G22–U9[f]	0.37	1.3	3.9	2.2

[a] Assignment of D_{HH} interactions observed in Fig. 1 (Addess et al. 1997)

[b] Ratio of the intensities of the cross and diagonal peaks observed in the 2D ^{1}H–^{1}H BEST-Jcomp-HMQC2 experiments. Uncertainties in the intensity ratios are the standard deviation calculated from triplicate experiments

[c] Experimental $\lvert D_{HH}\rvert$ values determined by fitting of the experimental intensity ratios using Eq. 1. $\Delta_1 = \Delta_2 = 35$ ms and $\lambda = 0.95$ (i.e., 95% H_2O/5% D_2O). Errors in D_{HH} are the standard deviation calculated from triplicate experiments

[d] Predicted $\lvert D_{HH}\rvert$ values from the RDC-refined structure of the IRE RNA (McCallum and Pardi 2003). The previously reported $^{1}D_{HN}$ values and solution structure (McCallum and Pardi 2003) were used as input for the REDCAT program (Valafar and Prestegard 2004) for SVD calculation of the alignment tensor. This tensor ($D_a^{NH} = -18.8$ Hz, $R = 0.16$, $\alpha = 24.1°$, $\beta = 108.4°$, and $\gamma = 123.7°$) was used along with the structure to then predict the D_{HH} values

[e] Internuclear distances determined from the RDC-refined solution structure of the IRE RNA (pdb entry 1NBR)(McCallum and Pardi 2003)

[f] Cross peaks between the imino protons of G22 and U9 were not observed in the two data sets collected at 500 MHz

Eq. 1 and Fig. 1). This overlap could be resolved by collecting the BEST-Jcomp-HMQC2 experiment as a 3D experiment with an additional ^{15}N dimension. With the exception of the G22–U9 wobble base pair, D_{HH} interactions are only observed between imino protons in the lower helical domain of the IRE RNA (Fig. 1). The largest D_{HH} values predicted between imino protons on neighboring base pairs in the lower helix were for G1–G2 (3.1 Hz) and G2–U27 (1.6 Hz), but were not observed. The G1–G2 interaction is not observed because of rapid base pair opening and exchange of the imino proton with water in the terminal base pair. The G2–U27 $\lvert D_{HH}\rvert$ value of 1.6 Hz is less than the smallest resolved interaction observed (1.9 Hz for G4–G25), and thus is below the sensitivity of the current data set. The predicted $\lvert D_{HH}\rvert$ values for other inter base pair interactions in the upper stem, G21–U9, G21–G22 and G21–U20, were all too small to observe (<1 Hz).

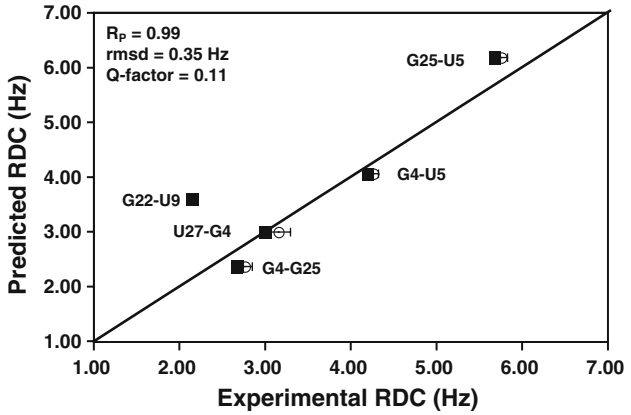

Fig. 2 Plot of the absolute value of the experimental and predicted imino ^{1}H–^{1}H RDCs of the IRE. The predicted RDCs were obtained from the previously RDC-refined solution structure of the IRE. The experimental imino $\lvert D_{HH}\rvert$ values for data collected at 600 MHz (filled squares) are shown along with the average $\lvert D_{HH}\rvert$ values determined from triplicate measurements at 500 MHz (open circles). The predicted RDCs were obtained using an alignment tensor of $D_a^{NH} = -18.8$ Hz, $R = 0.16$, $\alpha = 24.1°$, $\beta = 108.4°$, and $\gamma = 123.7°$ and the refined solution structure (McCallum and Pardi 2003) as input in REDCAT (Valafar and Prestegard 2004). Assignments for the $\lvert D_{HH}\rvert$ interactions are given for each point, and error bars on the average $\lvert D_{HH}\rvert$ values represent the standard deviation calculated from triplicate experiments. The Pearson's correlation coefficient, R_P, average rmsd and Q-factor (Cornilescu et al. 1998) for the 600 MHz data set are listed in the upper left-hand corner. These parameters were calculated without the $\lvert D_{HH}\rvert$ value for G22–U9 because of overlap of U9 and G21 imino proton resonances (see text)

The G4–U5 and G4–U27 interactions are of comparable volumes (2.70×10^7 and 2.58×10^7, respectively) in the NOESY spectrum (Fig. 3). These data indicate that G4–U5 and G4–U27 have similar distances between imino protons but that these interactions have different orientations with respect to the alignment tensor of the IRE. This is confirmed in Fig. 4, which highlights the ^{1}H–^{1}H interactions involving G4 in the NMR structure of the IRE (McCallum and Pardi 2003), where there are similar distances for the imino proton-imino proton interactions for G4–U5 and G4–U27 (Table 1), but where the

Additional structural information can be obtained in the IRE by comparing the BEST-Jcomp-HMQC2 spectrum (Fig. 1) with the ^{1}H–^{1}H NOESY spectrum (Fig. 3). For example, the G4 imino proton shows 3 cross peaks to imino protons of U5, G25 and U27 in the BEST-Jcomp-HMQC2 spectrum (boxed in Fig. 1). The G4–U5 interaction is the most intense of these (Fig. 1), has the largest ratio of intensities of cross peaks to diagonal peaks (Table 1) and therefore has a larger magnitude for D_{HH} (3.7 Hz) compared to what was observed for G4–U27 interaction (2.3 Hz). In contrast, the G4–U5 and G4–U27 crosspeaks

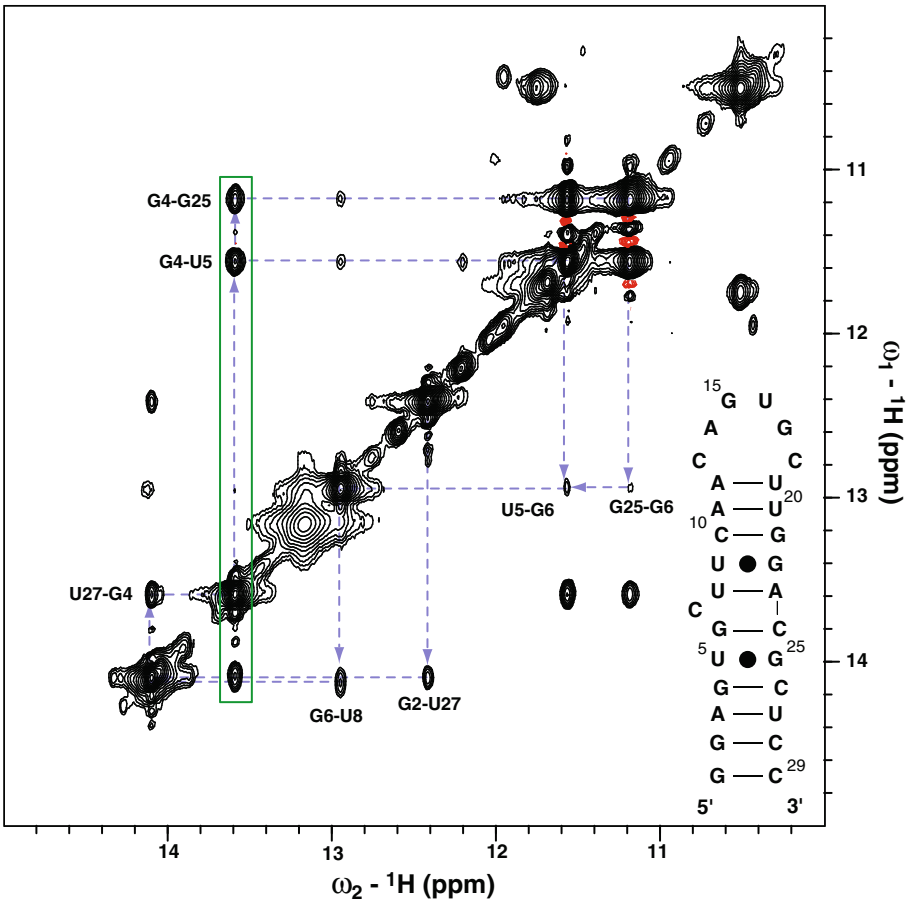

Fig. 3 Imino region of the 2D ^{1}H–^{1}H NOESY experiment with 175 ms mixing time collected on a 1 mM ^{15}N-labeled IRE containing ~17 mg/ml Pf1 phage. This spectrum was collected at 5°C on a Varian INOVA 600 MHz spectrometer equipped with a cryogenically cooled triple resonance *z*-axis probe. Water suppression was achieved with the gradient 11-echo scheme (Sklenár and Bax 1987). Black and red contour lines represent positive and negative intensity, respectively. Dashed blue lines show the imino proton walk in the lower helix, and the green box highlights the three cross peaks to the imino proton of G4

angles of these interactions differ giving rise to different RDC values. Thus, the ^{1}H–^{1}H RDCs for imino protons on neighboring base pairs complement the standard distance restraints obtained from NOESY data by providing information on the relative orientations of the observed interactions. Additionally, the imino ^{1}H–^{1}H RDCs from neighboring base pairs also complement one-bond imino ^{1}H–^{15}N intra-base RDCs, because the imino D_{HH} interactions will generally point along the helical axis; whereas, the imino D_{NH} vectors are generally perpendicular to the helix axis. Thus, the measurement of imino D_{HH} values represent a valuable target for additional restraints to be used in high-resolution structure determination and domain orientation studies of RNAs.

In some cases, the absence of an observable RDC can still provide structural information, especially when combined with ^{1}H–^{1}H NOESY data (Tjandra et al. 2000a, b). For example, some short through-space ^{1}H–^{1}H interactions that give rise to strong NOESY crosspeaks showed no cross peaks in DQF-COSY or TOCSY spectra of a partially aligned DNA duplex because the ^{1}H–^{1}H vectors are at angles that lead to very small RDCs (Hansen et al. 1998a, b). Thus, the ^{1}H–^{1}H RDC data yield orientational restraints that are not available from NOESY spectra. For the IRE data presented above, through-space correlations between imino protons in the upper helix were observed in the ^{1}H–^{1}H NOESY data, whereas the corresponding RDC correlations were all too small to detect in the BEST-Jcomp-HMQC2 spectra (<1 Hz). However, we observed an additional issue when comparing the 2D BEST-Jcomp-HMQC2 and NOESY spectra on the IRE. This is illustrated in the 1D spectra for the first t_1 value (Supplemental Fig. 2), where some imino resonances in the NOESY spectrum are not observed in the BEST-Jcomp-HMQC2 spectrum. These spectral differences cannot arise from solvent exchange because the NOESY experiment has a longer effective "mixing time" for solvent exchange than the BEST-Jcomp-HMQC2 experiment (~175 vs. ~70 ms). Thus, the differences in intensities of the imino resonance likely arise from differential multiple-quantum relaxation properties of imino groups during the constant time periods required for build-up of the ^{1}H–^{1}H RDCs in the BEST-Jcomp-HMQC2 experiment. This means it is not possible to directly compare sizes of cross peaks in the NOESY spectrum with those in the BEST-Jcomp-HMQC2 spectrum, and instead the magnitudes of the RDCs obtained from Eq. 1 need to be compared with the NOESY data.

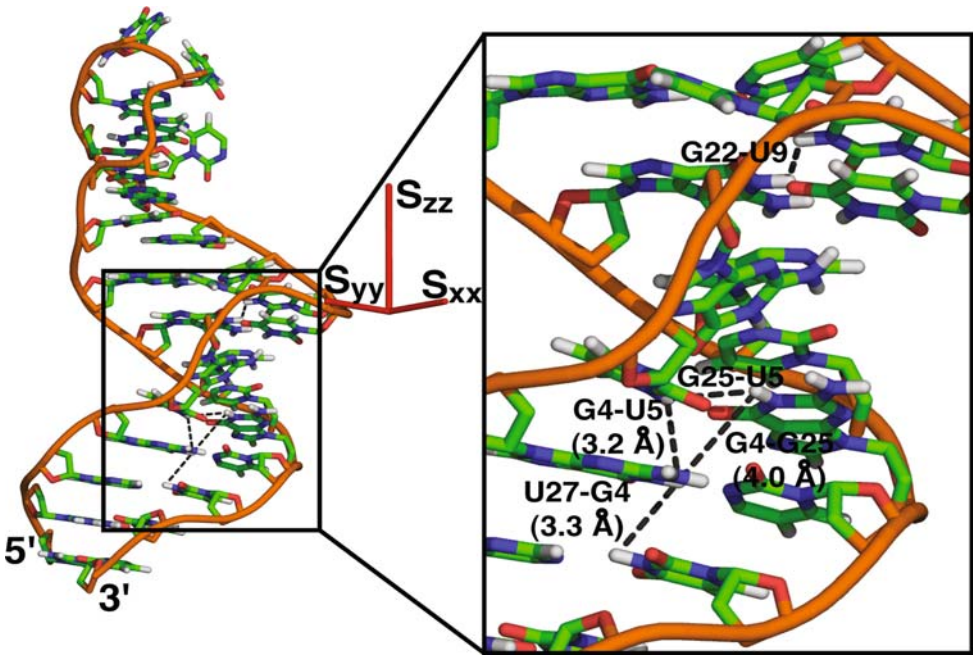

Fig. 4 Experimentally observed imino D_{HH} interactions are highlighted on the RDC-refined solution structure of the IRE (pdb entry 1NBR) (McCallum and Pardi 2003). The alignment tensor (red axis system) resulting from alignment in ~17 mg/ml Pf1 bacteriophage is shown next to the structure (McCallum and Pardi 2003). The lower stem containing some of the D_{HH} interactions is expanded highlighting dipolar interactions for G4 labeled with their respective inter-nuclear distances

Tjandra et al. (2000a) previously developed a protocol for incorporating ^1H–^1H RDCs into simulated annealing structure calculations, using the protein ubiquitin as a model system. This protocol employs an alignment tensor derived from one-bond RDCs, such as D_{NH} values, and an energy minimization procedure to find values of ^1H–^1H distance and orientation that satisfy the experimentally observed D_{HH} restraints. For ubiquitin, including the ^1H–^1H RDCs increased the accuracy and precision of the structure when compared to previous X-ray and NMR solution structures (Tjandra et al. 2000a). A similar protocol was also used to incorporate ^1H–^1H RDC restraints, measured between non-exchangeable protons, into the calculation of a high-resolution solution structure of the Dickerson dodecamer DNA (Tjandra et al. 2000b; Wu et al. 2003). These structure determinations utilized both the measured $|D_{HH}|$ and the absence of an observable ^1H–^1H RDC as restraints in the refinement (Tjandra et al. 2000a, b; Wu et al. 2003). Thus, the imino ^1H–^1H RDC data obtained here could be directly used in this type of high-resolution structure determination. Furthermore, the methods developed by Tjandra et al. (2000a) for incorporating ^1H–^1H RDC into structure refinements could also be used for domain orientation studies of RNAs.

Imino ^1H–^1H RDCs were also measured at 25°C on a 0.75 mM ^{15}N-labeled sample of native *E. coli* $tRNA^{Val}$ containing ~12 mg/ml Pf1 bacteriophage. HMQC constant time delays of 35 ms were employed using the same experimental parameters as described above for the IRE RNA. Only two sets of imino D_{HH} cross peaks were observed: between the imino protons of the G50–U64 wobble base pair and the imino protons of U29 and G42 in neighboring base pairs (Supplemental Fig. 3). A large imino D_{HH} was expected based on the short distance between the imino protons in a G–U wobble base pair (<2.4 Å). The cross and diagonal peak intensity ratio for the G50–U64 imino proton interaction is 3.31 which is >10-fold larger than the largest intensity observed in the IRE (G25 and U5, Table 1), corresponding to an experimental $|D_{HH}|$ value of ~49 Hz (Eq. 1, $\lambda = 0.90$). This experimental $|D_{HH}|$ value agrees well with the calculated value of 46.6 Hz derived from the previously described native *E. coli* $tRNA^{Val}$ model and alignment tensor ($D_a^{NH} = 20.4$ Hz, $R = 0.62$, $\alpha = 31.9°$, $\beta = 3.9°$, and $\gamma = -23.3°$) (Mollova et al. 2000; Vermeulen et al. 2005). The intensity ratio of the inter base pair U29–G42 interaction is 7.5×10^{-3} corresponding to a $|D_{HH}|$ value of 2.7 Hz (Eq. 1), which is much smaller than the predicted value of 8.4 Hz. However, both the U29 and G42 diagonal peaks are overlapped, leading to lower intensity ratios and therefore lower $|D_{HH}|$ values. In such cases of overlap, the constraints derived from these ^1H–^1H imino RDCs should take into account that the measured $|D_{HH}|$ represents only a lower limit, due to overestimate of the intensity of the diagonal peaks in Eq. 1. Additional ^1H–^1H imino RDCs were initially expected, so the imino D_{HH} were predicted using the previously determined $tRNA^{Val}$ model structure and Pf1 alignment tensor (Mollova et al. 2000; Vermeulen et al. 2005). However, many of the predicted imino D_{HH} interactions are too small to be observed in the BEST-Jcomp-HMQC2 experiment. In fact, after the U29–G42 interaction, the next largest $|D_{HH}|$ interaction occurs between the imino protons of G2–G3, G3–G4 and G52–G53 with predicted RDC values of ~3–4 Hz, and the

majority of the other predicted RDC values are <1 Hz. The very small ^{1}H–^{1}H RDCs arise because these imino ^{1}H–^{1}H interactions generally point along the helical axis and the orientation of the two helical regions of this tRNA with respect to the alignment tensor is unfavorable for these RDCs (Mollova et al. 2000; Vermeulen et al. 2005). Since, both helices are oriented in a manner that only small imino ^{1}H–^{1}H RDCs are observed, this information could still be used to help determine the global structure of this RNA. One issue that also needs to be considered when interpreting the absence of observable ^{1}H–^{1}H RDC interactions is that the larger size of $tRNA^{Val}$ (76 nucleotides) leads to faster multiple-quantum relaxation during the two HMQC periods, which reduces the sensitivity of the BEST-Jcomp-HMQC2 experiment.

One method for increasing the relative size of cross peaks in the BEST-Jcomp-HMQC2 experiment is to use a higher degree of molecular alignment. Thus the BEST-Jcomp-HMQC2 experiment was also performed on a ^{15}N-labeled sample of *E. coli* $tRNA^{Val}$ containing ~25 mg/ml Pf1 phage. However, this higher degree of alignment resulted in very broad lines in the direct ^{1}H dimension, which arise from the large imino proton to amino proton dipolar couplings. Therefore, higher alignment can actually reduce the signal-to-noise in the BEST-Jcomp-HMQC2 experiment. A second approach for increasing the relative size of the cross peaks in the BEST-Jcomp-HMQC2 experiment is to increase the two constant time delays in the two HMQC periods (Δ_1 and Δ_2 in Supplemental Fig. 1), which allows more time for smaller couplings to evolve. Thus, a 2D ^{1}H–^{1}H BEST-Jcomp-HMQC2 experiment was acquired on the IRE at 500 MHz varying the HMQC constant time delays from 30 to 60 ms. As expected from Eq. 1, the ratio of the cross peaks and diagonal peaks increases with longer Δ delays; however, the signal-to-noise decreases because of increased multiple quantum relaxation. In fact, the weak cross peaks observed between imino resonances G4 and G25 in Fig. 1 were no longer observed in the 60 ms constant time spectrum (data not shown). Thus, no new D_{HH} interactions were observed with the 60 ms constant time periods.

Finally, to test the effect of the BEST methodology (Schanda et al. 2007) for measurement of imino ^{1}H–^{1}H RDCs, the spectrum obtained with the BEST-Jcomp-HMQC2 pulse sequence (Supplementary Fig. 1) was compared with a spectrum obtained using the original semi-selective HMQC2 pulse sequence (Wu and Bax 2002). The SS-HMQC experiment was acquired at 500 MHz on the IRE with the same number of complex points in each dimension as the BEST experiment, but with a longer inter-scan delay (1.6 vs. 0.8 s) and fewer scans per FID (144 vs. 256) resulting in the same total experiment time (20 h). For the SS-HMQC experiment, D_{HH} interactions were observed for all of the imino proton-imino proton interactions except G22–U9. However, for the peaks observed in both the BEST and SS-HMQC2 experiments collected at 500 MHz, the average increase in signal intensity is ~3.5-fold when the BEST methodology is utilized. This ~3.5-fold signal increase is higher than the ~1.8-fold increase predicted from the difference in the number of scans collected in each experiment (256 vs. 144). For example, Fig. 5 compares 1D traces through the

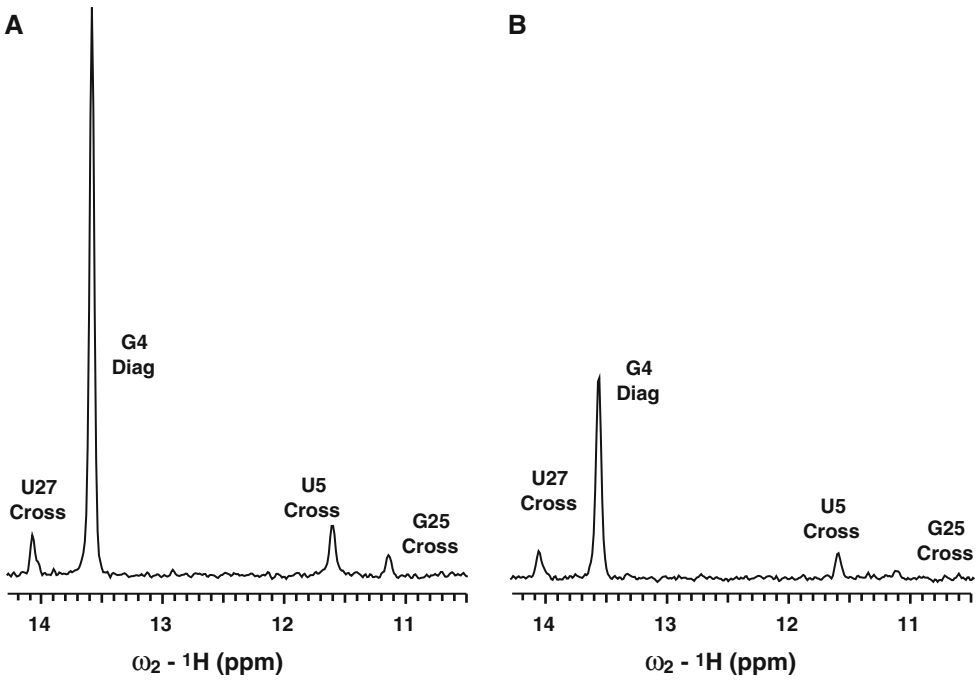

Fig. 5 1D traces for the G4 imino resonance taken from the 2D (**a**) BEST-Jcomp-HMQC2 and (**b**) SS-HMQC2 spectra on the IRE in Pf1 bacteriophage. Both spectra were collected at 500 MHz and 25°C for ~20 h, as described in the text. The assignments for G4 diagonal peak and U27, U5 and G25 cross peaks are given

G4 imino resonance for the BEST and SS-HMQC2 spectra, illustrating that the G25–G4 cross peak is barely observable in the SS-HMQC2 experiment. Thus, the longitudinal relaxation enhancement afforded by the BEST methodology leads to an increase in signal-to-noise.

It is demonstrated here that accurate imino proton-imino proton $|D_{HH}|$ values can be obtained using the BEST-Jcomp-HMQC2 experiment collected on partially aligned RNA samples. Interactions were observed between the imino protons in G–U wobble base pairs as well as between the imino protons of neighboring base pairs in the 29 nucleotide IRE RNA and 76 nucleotide native *E. coli* $tRNA^{Val}$. These RDC data complement standard NOESY distance restraints due to their additional dependence on the relative orientation of the internuclear interactions to the common alignment frame. The D_{HH} data also provide complementary orientation information to the imino $^{1}H–^{15}N$ RDCs, since the imino $^{1}H–^{1}H$ RDC generally point along the helical axis whereas the imino $^{1}H–^{15}N$ RDCs generally point perpendicular to the helical axis. Therefore, these imino D_{HH} restraints contain valuable information for domain orientation studies of RNAs.

Acknowledgements We thank Dr. J. Boisbouvier for providing the original pulse sequence and Dr. A. Bax for valuable discussions. This work was supported in part by NIH grant AI33098, and MPL was supported in part by a NIH training grant T32 GM65103. The NMR instrumentation was purchased with partial support from NIH grant RR11969 and NSF grants 9602941 and 0230966.

References

Addess KJ, Basilion JP, Klausner RD, Rouault TA, Pardi A (1997) Structure and dynamics of the iron responsive element RNA: implications for binding of the RNA by iron regulatory binding proteins. J Mol Biol 274:72–83

Al-Hashimi HM, Gosser Y, Gorin A, Hu WD, Majumdar A, Patel DJ (2002) Concerted motions in HIV-1 TAR RNA may allow access to bound state conformations: RNA dynamics from NMR residual dipolar couplings. J Mol Biol 315:95–102

Bax A, Kontaxis G, Tjandra N (2001) Dipolar couplings in macromolecular structure determination. Methods Enzymol 339:127–174

Boisbouvier J, Delaglio F, Bax A (2003) Direct observation of dipolar couplings between distant protons in weekly aligned nucleic acids. Proc Natl Acad Sci USA 100:11333–11338

Bondensgaard K, Mollova ET, Pardi A (2002) The global conformation of the hammerhead ribozyme determined using residual dipolar couplings. Biochemistry 41:11532–11542

Bothner-By AA, Domaille PJ, Gayathri C (1981) Ultra-high-field NMR spectroscopy-Observation of proton-proton dipolar coupling in paramagnetic bis[Tolyltris(Pyrazolyl)Borato]Cobalt(II). J Am Chem Soc 103:5602–5603

Cornilescu G, Marquardt JL, Ottiger M, Bax A (1998) Validation of protein structure from anisotropic carbonyl chemical shifts in a dilute liquid crystalline phase. J Am Chem Soc 120:6836–6837

D'Souza V, Dey A, Habib D, Summers MF (2004) NMR structure of the 101-nucleotide core encapsidation signal of the Moloney murine leukemia virus. J Mol Biol 337:427–442

Davis JH, Tonelli M, Scott LG, Jaeger L, Williamson JR, Butcher SE (2005) RNA helical packing in solution: NMR structure of a 30 kDa GAAA tetraloop-receptor complex. J Mol Biol 351:371–382

Fiala R, Munzarova ML, Sklenar V (2004) Experiments for correlating quaternary carbons in RNA bases. J Biomol NMR 29:477–490

Getz M, Sun XY, Casiano-Negroni A, Zhang Q, Al-Hashimi HM (2007) NMR studies of RNA dynamics and structural plasticity using NMR residual dipolar couplings. Biopolymers 86:384–402

Hansen MR, Mueller L, Pardi A (1998a) Tunable alignment of macromolecules by filamentous phage yields dipolar coupling interactions. Nat Struct Biol 5:1065–1074

Hansen MR, Rance M, Pardi A (1998b) Observation of long-range $^{1}H–^{1}H$ distances in solution by dipolar coupling interactions. J Am Chem Soc 120:11210–11211

Hansen MR, Hanson P, Pardi A (2000) Filamentous bacteriophage as a versatile method for aligning RNA, DNA and proteins for measurement of NMR dipolar coupling interactions. Methods Enzymol 317:220–240

Kung HC, Wang KY, Goljer I, Bolton PH (1995) Magnetic alignment of duplex and quadruplex DNAs. J Magn Reson B 109:323–325

Latham MP, Brown DJ, McCallum SA, Pardi A (2005) NMR methods for studying the structure and dynamics of RNA. ChemBioChem 6:1492–1505

Lipsitz RS, Tjandra N (2004) Residual dipolar couplings in NMR structure analysis. Ann Rev Biophys Biomol Struct 33:387–413

Lukavsky PJ, Kim I, Otto GA, Puglisi JD (2003) Structure of HCV IRES domain II determined by NMR. Nat Struct Biol 10:1033–1038

McCallum SA, Pardi A (2003) Refined solution structure of the iron-responsive element RNA using residual dipolar couplings. J Mol Biol 326:1037–1050

Meier S, Haussinger D, Jensen P, Rogowski M, Grzesiek S (2003) High-accuracy residual H-1(N)-C-13 and H-1(N)-H-1(N) dipolar couplings in perdeuterated proteins. J Am Chem Soc 125:44–45

Mollova ET, Pardi A (2000) NMR solution structure determination of RNAs. Curr Opin Struct Biol 10:298–302

Mollova ET, Hansen MR, Pardi A (2000) Global structure of RNA determined with residual dipolar couplings. J Am Chem Soc 122:11561–11562

Pervushin K, Vogeli B, Eletsky A (2002) Longitudinal H-1 relaxation optimization in TROSY NMR spectroscopy. J Am Chem Soc 124:12898–12902

Prestegard JH, Bougault CM, Kishore AI (2004) Residual dipolar couplings in structure determination of biomolecules. Chem Rev 104:3519–3540

Schanda P, Brutscher B (2005) Very fast two-dimensional NMR spectroscopy for real-time investigation of dynamic events in proteins on the time scale of seconds. J Am Chem Soc 127:8014–8015

Schanda P, Kupce E, Brutscher B (2005) SOFAST-HMQC experiments for recording two-dimensional heteronuclear correlation spectra of proteins within a few seconds. J Biomol NMR 33:199–211

Schanda P, Lescop E, Falge M, Sounier R, Boisbouvier J, Brutscher B (2007) Sensitivity-optimized experiment for the measurement of residual dipolar couplings between amide protons. J Biomol NMR 38:47–55

Scott LG, Tolbert TJ, Williamson JR (2000) Preparation of specifically H-2- and C-13-labeled ribonucleotides. Methods Enzymol 317:18–38

Sklenár V, Bax A (1987) Spin-echo water suppression for the generation of pure-phase two-dimensional NMR spectra. J Magn Reson 74:469–479

Tian F, Fowler CA, Zartler ER, Jenney FA, Adams MW, Prestegard JH (2000) Direct measurement of H-1-H-1 dipolar couplings in proteins: a complement to traditional NOE measurements. J Biomol NMR 18:23–31

Tjandra N, Bax A (1997) Direct measurement of distances and angles in biomolecules by NMR in a dilute liquid crystalline medium. Science 278:1111–1114

Tjandra N, Marquardt J, Clore GM (2000a) Direct refinement against proton-proton dipolar couplings in NMR structure determination of macromolecules. J Magn Reson 142:393–396

Tjandra N, Tate S, Ono A, Kainosho M, Bax A (2000b) The NMR structure of a DNA dodecamer in an aqueous dilute liquid crystalline phase. J Am Chem Soc 122:6190–6200

Tolman JR, Flanagan JM, Kennedy MA, Prestegard JH (1995) Nuclear magnetic dipole interactions in field-oriented proteins-information for structure determination in solution. Proc Natl Acad Sci USA 92:9279–9283

Valafar H, Prestegard JH (2004) REDCAT: a residual dipolar coupling analysis tool. J Magn Reson 167:228–241

Vermeulen A, Zhou HJ, Pardi A (2000) Determining DNA global structure and DNA bending by application of NMR residual dipolar couplings. J Am Chem Soc 122:9638–9647

Vermeulen A, McCallum SA, Pardi A (2005) Comparison of the structure and dynamics of native and unmodified $tRNA^{val}$. Biochemistry 44:6024–6033

Wu Z, Bax A (2002) Measurement of long-range ^{1}H–^{1}H dipolar couplings in weakly aligned proteins. J Am Chem Soc 124: 9672–9673

Wu Z, Delaglio F, Tjandra N, Zhurkin VB, Bax A (2003) Overall structure and sugar dynamics of a DNA dodecamer from homo- and heteronuclear dipolar couplings and 31P chemical shift anisotropy. J Biomol NMR 26:297–315

Ying J, Grishaev A, Latham MP, Pardi A, Bax A (2007) Magnetic field induced residual dipolar couplings of imino groups in nucleic acids from measurements at a single magnetic field. J Biomol NMR 39:91–96